CrossMark

Comparison of HIPIMS sputtered Ag- and Cu-surfaces leading to accelerated bacterial inactivation in the dark

Sami Rtimi [a], Oualid Baghriche [a], Cesar Pulgarin [a,**], Arutiun Ehiasarian [b], Ralf Bandorf [c], John Kiwi [d,*]

[a] Ecole Polytechnique Fédérale de Lausanne, EPFL-SB-ISIC-GPAO, Station 6, CH-1015, Lausanne, Switzerland
[b] Sheffield Hallam Univ, Howard St, Sheffield, S1 1WB, UK
[c] Fraunhofer-Institute for Surface Engineering and Thin Films (IST), Bienroder Weg 54E, 38108 Braunschweig, Germany
[d] Ecole Polytechnique Fédérale de Lausanne, EPFL-SB-ISIC-LPI, Bat Chimie, Station 6, CH1015, Lausanne, Switzerland

ARTICLE INFO

ABSTRACT

Recently, compact uniform and adhesive films of Ag and Cu have been prepared by DC-magnetron sputtering (DC), pulsed DC magnetron sputtering (DCP) and high power impulse magnetron sputtering (HIPIMS). This study reports the HIPIMS deposition for Ag and Cu on textile fabrics, the bacterial inactivation kinetics and the nature of the species in the plasma produced during HIPIMS sputtering. The deposition rates of Ag and Cu atoms and the bacterial inactivation times are reported in the dark and under light as a function of the applied peak currents during the sputtering by HIPIMS. By X-ray photoelectron spectroscopy (XPS), the surface percentage atomic concentration and the oxidation state changes are reported during bacterial inactivation. The Ar and metal-ions produced in the magnetron chamber were determined by mass spectroscopy (QMS). A mechanism for the bacterial inactivation is suggested for Ag and Cu HIPIMS sputtered surfaces.

© 2014 Elsevier B.V. All rights reserved.

1. Introduction

The ambient contamination by biofilms spreading bacteria for long times in hospitals, schools and many public places requires the preparation of adhesive antibacterial/fungi thin films showing rapid biocidal kinetics. Antimicrobial nanoparticulate film preparation is a topic of increasing attention since they can reduce/eliminate the formation of infectious bacteria biofilms leading to hospital acquired infections (HAI) [1]. The microbes causing HAI have two properties: many of them are toxic/resistant to antibiotics and they survive on hospital surfaces for long times [2]. These nosocomial infections due to antibiotic resistant bacteria are becoming more frequent during the last decade and contribute to the increasing of hospital care costs. The level of contamination of public hospitals in the UK and Switzerland has been found to be higher than the allowed level set for hospital rooms. For example, the contamination of 10^5 CFU/cm^2 was observed in a diabetic wound dressing. But in the vicinity of the patient, a microbial density of 10^2 CFU/cm^2 was found. Disinfecting surfaces were applied and strongly decrease the microbial density, since bacterial concentration was not high and re-growth of bacteria was not observed [3]. This observation warrants the investigation of antibacterial surfaces as addressed in the present study.

Colloidal deposition of surfaces, like textiles and other materials is applied widely to prepare disinfectant/antibacterial materials. In our laboratory Ag-colloids were reduced by isopropanol and precipitated by ammonia on the textile surface inducing bactericide behaviour [4]. In a further study, Ag-colloids were fixed on cotton to investigate their antibacterial kinetics in the dark [5]. Antibacterial Cu-colloid loading textile surfaces have been reported leading to efficient antibacterial activity [6,7]. The colloid or sol–gel preparation deposited films are not mechanically stable, nor reproducible, and present low uniformity and little adhesion since they can be wiped off by a cloth or thumb [8]. This moved us to work on the sputtering of antibacterial films to overcome the shortcomings of colloidal loaded films. The HIPIMS sputtered films presenting a progress compared to films sputtered by more traditional approaches like DC and DCP. CVD/PDV deposition methods present some disadvantages and this will be discussed in the next paragraph. The problem to fix colloids on surfaces encountered during CVD deposition is in connection with the heat needed for the film fixation on the substrate. This has to be resistant to heat. Deposition by sputtering of metal/oxides/semiconductors on non-heat resistant substrates is possible since the polymer thin films, textiles and plastics can be heated at temperatures up to 150 °C.

In a typical CVD process, the substrate is exposed to the volatile precursors. Due to the applied heat the precursor decomposes on the substrate surface depositing amorphous/polycrystalline coatings. The volatile species condense on the substrate having a lower temperature. The disadvantages of conventional PVD deposition approach are: the high investment costs and the high temperatures needed precluding

film deposition on textiles besides the large amount of heat used requiring costly cooling systems. Recently, Foster et al. [9], Yates et al. [10], Musil et al. [11], and Brooks et al. [12] have reported antibacterial Ag and Cu coatings on glass and polymer films depositing the metal/oxides by CVD.

Ag-nanoparticles exhibit bacterial and fungicidal properties. They can accumulate on the cell wall of bacteria and release Ag-ions that due to their small size penetrate into the cells through the wall porins [13]. Ag-nanoparticles affect the bacteria respiratory enzyme due to the production of ROS and associated DNA damage leading to death [14]. The release of Ag-ions from Ag-grafted surfaces involves Ag-oxidation reactions due to the oxygen available to the Ag-clusters, protons, and salts and is directly dependent on the Ag-particle size that for large particles is effective only when releasing Ag-ions in sufficient concentrations and in a sustained way over long time periods [15].

The field of antibacterial Cu-film preparation and evaluation has gained much attention during the last decade since they have been reported to be effective in reducing hospital-acquired infections (HAI) [16]. Since the effect of Cu-ions is extremely toxic to bacteria at very low concentrations (ppb range) many formulations of surfaces and implants coated with Cu present a higher cytocompatibility than Ag for *mammalian* cells. Cu is a metabolizable agent [17] compared to Ag that stays in the body after ingestion increasing the Ag-serum levels [18]. The antibacterial effects of Cu–TiO_2 coatings against MRSA have been reported by Cu–TiO_2 coating thickness, the layers on medical devices showing high mechanical stability without cracks in the coating [19]. The area of sputtering on medical devices is a current area of research. Hashimoto et al. [20] have reported the preparation of the Cu and TiO_2/Cu films by sol–gel methods presenting bactericide action under visible light. Further colloidal Cu-coated textiles showing antibacterial properties have been prepared and tested in our laboratory [21,22]. The particular interest in Cu-textiles is based on the fact that the porous hydrophilic structure of textiles provides a suitable environment for bacterial growth. Cu-nanoparticles have shown recently to produce strong antibacterial effects in textiles designed for medical applications [6,7].

The improvement in the performance and utility of Ag and Cu antibacterial films is to produce a film microstructure inducing an accelerated bacterial inactivation concomitant with toxicity below the accepted standards set for its use in medical applications [23]. The film uniformity, stable structure and adhesive properties are currently under investigation by academic institutions and pharma/biotechnology companies producing devices for medical device implants covered with antibacterial coatings [24]. The regular, periodic and continuous elution of antibiotics and antiseptics (or both) added on medical devices and implants over long period of times is the central problem to avoid infections that lead to the replacement of the implants after some time. HIPIMS sputtered devices/surfaces with Ag, Cu or both eluting Ag-ions and Cu-ions over long times could be a solution to this problem and need a long term testing by ion coupled mass spectrometry (ICP-MS), X-ray fluorescence (XRF) and XPS. The long-term testing for the elusive properties of the Ag, Cu HIPIMS surface is under way in our laboratory and will be reported elsewhere at a later date.

HIPIMS generates high-density plasma ionizing the metal to a high degree at low pressures avoiding the formation of macro-particles that deteriorate the properties of the growing film. The development of HIPIMS in the last decade is due to the growing demand for high quality anticorrosive films in aircraft, car industry and other industrial sectors. Recently, high power pulsed magnetron sputtering (HIPIMS) has gained increasing attention as a more advanced sputtering method to deposit uniform, robust films onto a variety of substrates. This is due to the high pulse power densities of several kW leading to elimination of growth defects and concomitant densification of the sputtered films [25]. The enhanced densification attained by sputtering with HIPIMS is due to the high ion-to neutral-ratio found in the plasma during the deposition process compared to more traditional forms of sputtering. In conventional DC-sputtering, the degree of ionization is 1%–5% and the electronic density ~10^{14} e$^-$/m^3. The majority of the particles reaching the substrate are made up of Ar-ions [26]. In DCP-sputtering, the electronic density ~10^{16} e$^-$/m^3 and the ionization are higher compared to DC. In the case of HIPIMS, pulses from one microsecond up to milliseconds generate current densities of ~10^{18} e$^-$/m^3 which is 10^4 times higher than that obtained with conventional DC-sputtering and the degree of ionization reaches about 50–80% [27–30]. Improvement in the film homogeneity is achieved by HIPIMS as a consequence of the high ion-fraction of the sputtered metal(s). Until now, the use of DC, pulse sputtering (DCP) and HIPIMS sputtering to deposit bactericide metal nanoparticles films precluding bacterial inactivation has not been widely investigated for the large scale production of hospital personnel (clothing), bedding textiles, towels, curtains, chairs, floors, and medical implants.

2. Experimental section

2.1. HIPIMS-sputtering on polyester, materials, film thickness calibration and XRF evaluation of Ag and Cu

The HIPIMS deposition of metals was carried out in a CMS-18 vacuum system from Kurt Lesker Ltd. evacuated to 10^{-5} Pa by a turbomolecular pump [31]. Fig. 1 shows the scheme of the HIPIMS chamber. The Cu-target was 5 cm in diameter, 99.99% pure from K. Lesker Ltd. UK. The mass spectrometry measurements were carried out in a Hiden Analytical Ltd PSM003 unit to determine the ion-composition of the ions in the plasma Ar-atmosphere [32]. The HIPIMS was operated at 100 Hz with pulses of 100 ms separated by 10 ms. The HIPIMS short pulses avoid a glow-to-arc transition during plasma particle deposition.

The polyester used corresponds to the EMPA test cloth sample No 407. It is a polyester Dacron, type 54 spun, plain weave ISO 105-F04 used for color fastness determinations. The metal content on the substrates was evaluated by X-ray fluorescence (XRF). The spectrometer used was RFX, PANalytical PW2400.

2.2. Escherichia coli and MRSA counting method during bacterial inactivation

The samples of *Escherichia coli* (*E. coli K12*) was obtained from the Deutsche Sammlung von Mikroorganismen und Zellkulturen GmbH (DSMZ) ATCC23716, Braunschweig, Germany, to test the antibacterial activity of the Ag and Cu sputtered samples. The 100 μL culture aliquots with an initial concentration of ~10^6 CFU mL^{-1} in NaCl/KCl (pH 7) were placed on coated and uncoated (control) polyethylene fabric. A well-
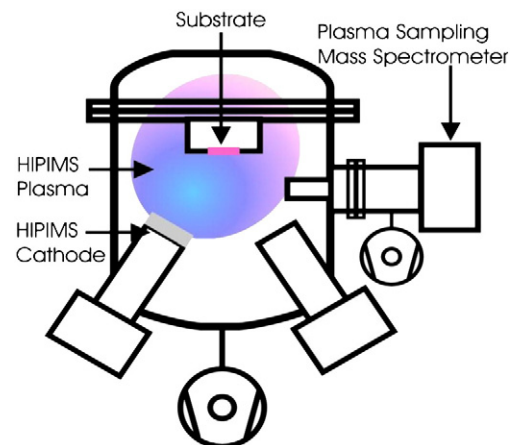

Fig. 1. Schematic of the HIPIMS sputtering unit used for the sputtering of substrates.

dispersed non-heterogeneous contact is established between the sample and the bacterial solution. 100 μL of the E. coli solution was contacted with the TiO2 uniform films. The distribution of bacteria on the substrate turned out to be homogeneous and was in a position to contact the inoculated cells on contact. The exposition was done at ambient temperature. The samples were then placed on Petri dishes provided with a lid to prevent evaporation. After each determination, the fabric was transferred into a sterile 2 mL Eppendorf tube (900 μL) autoclaved NaCl/KCl saline solution. This solution was subsequently mixed thoroughly using a vortex for 3 min. Serial dilutions were made in NaCl/KCl solution. A sample of 100 μL of each CFU run was pipetted onto a nutrient agar plate and then spread over the surface of the plate using the standard plate method. Agar plates were incubated lid down, at 37 °C for 24 h before colonies were counted. Three independent assays were done for each sputtered sample. The CFU statistical analysis was performed calculating the standard deviation values. The average values were compared by one-way analysis of variance and with the value of statistical significance. The one-way analysis of variance (one-way ANOVA) was used to compare the mean of the samples using the Fisher distribution. The response variable was approximated for the sample data obtained from the photocatalytic inactivation of test samples presenting the same distribution within the same sputtering time.

The Staphylococcus aureus strain used for this study was the MRSA ATCC 43300 strain. Bacteria were stored at −80 °C. Overnight cultures for bacterial inoculate were prepared in brain heart infusion (BHI) media (OXOID, Basingstoke, UK) from a single colony picked on a BHI agar plate and incubated at 37 °C for 16 h. The inoculation of polyester fabrics was performed in the following way: squares of polyester and Cu-sputtered polyester were inoculated with 10^7 CFU. After the inoculation, samples were placed in a humidified chamber and the viability of the bacteria was assessed at several times. The inoculated coupons were placed in a 2 mL Eppendorf containing 1 mL NaCl 0.9% and bacteria were detached by vortexing (3 min). Bacterial counts were performed by plating the re-suspended bacteria on BHI agar-plates [33].

2.3. ICP-MS during bacterial inactivation and mass spectroscopy (QMS) of samples

Inductively coupled plasma spectrometry (ICP-MS) was used to determine the Cu since it is a sensitive analytical technique due to the low background and high ion transmission. The Finnigan™ ICPS used was equipped with a double focusing reverse geometry mass spectrometer with a resolution of 1.2×10^5 cps/ppb and a detection limit of 0.2 ng/L. Samples 1 cm^2 were placed in Eppendorf tubes containing 1 mL (NaCl/KCl 0.08% solution). The solutions were then diluted 10 times to reach the volume necessary for the ICP-MS analyses.

The mass spectrometry measurements were carried out in a Hiden Analytical Ltd PSM003 unit attached to the sputtering unit to determine the ion-composition of the ions in the Ar-plasma at different currents [32].

2.4. X-ray photoelectron spectroscopy of Ag, Cu-films (XPS)

An AXIS NOVA photoelectron spectrometer (Kratos Analytical, Manchester, UK) equipped with monochromatic AlK$_\alpha$ ($h\nu = 1486.6$ eV) anode was used. The electrostatic charge effects on the samples were compensated by means of the low-energy electron source working in combination with a magnetic immersion lens. The carbon C1s line with position at 284.6 eV was used as a reference to correct the charging effect. The quantitative surface atomic concentration of some elements was determined from peak areas using sensitivity factors [34,35]. Spectrum background was subtracted/corrected for electrostatic charging according to Shirley [36]. The XPS spectra for the Cu-species were analyzed by means of spectra deconvolution software (CasaXPS-Vision 2, Kratos Analytical UK).

3. Results and discussion

3.1. Film thickness calibration and determination of metal-content

Fig. 2 presents the nominal calibration of the Ag-thin coating attained by HIPIMS for currents 1, 2 and 5 A. Taking the lattice distance between Ag-atoms as 0.3 nm [37] a monolayer of Ag is estimated to have a density of 10^{15} atoms/cm^2. HIPIMS sputtering at 2 A deposited a coating ~100 nm thick after 160 s. It follows that in one second, a layer of 0.62 nm was deposited and if each atomic layer is taken as 0.2 nm thick, then a rate of deposition of ~3 layers per second was deposited equivalent to a silver deposition rate of 3×10^{15} atoms/cm^2 s. Table 1 presents the Ag wt.%/wt. polyester and the thickness of the Ag-layers deposited by HIPIMS at different times.

The calibration of the Cu-nanoparticulate film thickness by HIPIMS on the Si-wafers is shown in Fig. 3. The thicknesses of the Cu-loading of the Cu-films sputtered by HIPIMS are shown in Table 2. The calibration reported in Fig. 3 presented a 10–15% experimental error. The 20 s HIPIMS deposition time with 6 A led to a film thickness of 28 nm. With 60 Amps a 28 nm layer was deposited (see Fig. 3) within 60 s equivalent to 140 layers with a content of 1.4×10^{17} atoms Cu/cm^2. This is a deposition ratio for Cu of 2.3×10^{15} atoms/cm^2 s.

3.2. E. coli inactivation kinetics and mechanism on Ag-polyester

Fig. 4 presents the bacterial inactivation kinetics for Ag-polyester fabrics sputtered by HIPIMS at 5 A. This is the most suitable sample leading to a bacterial inactivation within 2 h requiring a sputtering time of 75 or 150 s.

Fig. 5 shows the bacteria inactivation times as a function of the nominal thickness of the Ag-layers deposited by HIPIMS at 5 A and the layers deposited by direct current magnetron sputtering (DCMS) at 0.3 A. Fig. 5 shows the significant savings of Ag and sputtering times by HIPIMS compared with the more traditional DCMS. Generally, one would expect more compact, denser metal films for HIPIMS to present reduced antibacterial efficacy. The results in Fig. 5 show the opposite effect. This can be explained by local softening of the polymer and possible void formation during the first stage of film growth on polymers due to the local higher temperatures available in the magnetron chamber during HIPIMS sputtering.

Ag samples in the dark by contact with ambient air containing water-vapor $(H_2O)_v$ deposit AgOH on its surface. The favorable decomposition of AgOH leads to Ag_2O as in (Eq. 1)

$$AgOH \rightarrow Ag_2O + H_2O \ (pk = 2.87) \tag{1}$$

Ag_2O is thermodynamically stable at pH 6–7 and leads to the bacterial inactivation of E. coli shown in Fig. 4. The hydrolysis and equilibrium
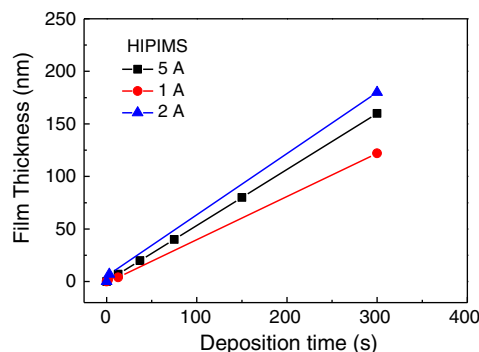

Fig. 2. Nominal calibration of the Ag thickness attained by HIPIMS for currents 1, 2 and 5 A.

Table 1
HIPIMS sputtering of Ag, relationship of HIPIMS sputtering time, the % Ag wt./wt. polyester and Ag film thicknesses at 1, 2 and 5 A.

HIPIMS	Time (s)	% Ag wt./wt.	Ag film thickness nm
1 A	2	0.002	2
1 A	13	0.003	4
2 A (2)	3	0.014	7
HIPIMS 5 A	Time (s)	% Ag wt./wt.	Thickness nm
(2)	13	0.0029	7
(3)	37	0.0086	20
(4)	75	0.0315	40
(5)	150	0.0630	80

Table 2
Sputtering time, thickness and % Cu wt./wt. of the Cu-layers sputtered by HIPIMS on polyester at 6 and 60 Amps.

	Deposition time [s]	[Amps]	Thickness [nm]	Cu [%-wt.]
HIPIMS	2	6	1.5	0.0121
	4	6	4	0.0200
	18	6	16	0.0600
	21	6	28	0.1120
	3	60	1.5	0.0073
	7	60	.3	0.0182
	35	60	16	0.0675
	61	60	28	0.1020

of Ag_2O have been reported [39]. Visible/actinic light irradiation photo-activates Ag_2O with $1.46 < bg < 2.25$ eV as noted next in Eq. (2)

$$Ag_2O + light \rightarrow Ag_2O\left(h^+\right) + Ag_2O\left(e^-\right) \qquad (2)$$
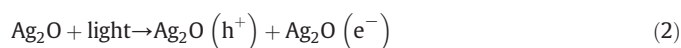
The Ag_2O in Eqs. ((1)–(2)) reacts with e^- induced by light irradiation Eq. (3)

$$Ag_2O + e^- \rightarrow Ag^o + O_2 \qquad (3)$$

The O_2 shown in Eq. (3) promotes reactions (5,6) producing highly oxidative radicals, while the h^+ in Eq. (2) reacts with H_2O in Eq. (4). This reaction runs parallel with Eq. (5) generating OH^o radicals (or other highly reactive oxidative radicals) able to inactivate *E. coli*. The h^+ in Eq. (2) reacts with water-vapor leading to radical species

$$h^+ + H_2O \rightarrow OH^o + H^+ \qquad (4)$$

and the e^- in Eq. (2) reacts with water-vapor in the air (O_2) leading also to radical species

$$e^- + H_2O + O_2 \rightarrow OH^o + OH^- \qquad (5)$$

The silver nanoparticulate films exhibit the Volmer–Weber growth mechanism that assumes an island-by-island growth because of the large cohesive forces existing among the Ag-atoms. The strong coalescence of Ag after deposition allows the Ag-islands to grow into a nanoparticulate film as already reported for DCMS sputtered films [26,38] (Figs. 3 and 6). The interest in HIPIMS deposition of Ag is that the thin film $n < 100$ nm contains $Ag/Ag_2O/AgO$ effective in inactivating pathogens [3,23,24].

3.3. E. coli inactivation kinetics and mechanism on Cu-polyester and redox catalysis

Fig. 6a presents the inactivation kinetics of *E. coli* on Cu-polyester HIPIMS sputtered for 3 s and 60 s at 60 Amps. It is readily seen that at longer HIPIMS sputtering times, the 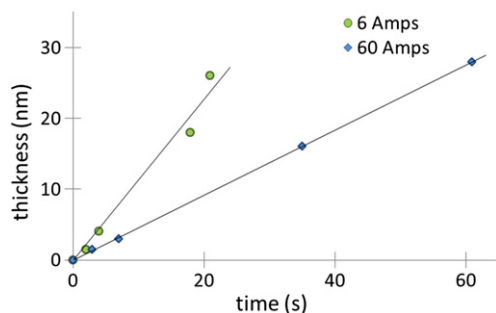inactivation time for *E. coli* becomes shorter. A local softening of the fibers at the contact sites with Cu may play a significant role in the inactivation time of *E. coli* due to the effect of higher temperatures available to the substrate [25,26]. The Cu-atoms diffuse anisotropically on the textile surface and the diffusion is driven by the high energy given to the Cu-ions. The high energy given to the Cu-ions is partly released when the Cu-ions arrive at the polyester surface and contact with surface electrons or bond with the textile surface [37].

Fig. 6b shows the release of Cu-ions inactivating *E. coli* as a function of catalyst recycling up to the 8th cycle by ICP-MS. The release of Cu^- from the TiO_2/Cu samples shown in Fig. 6b was ~8 ppb/cm^2. This value is lower compared to the Cu-release from the Cu-HIPIMS sputtered samples of to ~18 ppb Cu/cm^2 at the end of the 8th cycle. In both cases the amounts of Cu are not to be cytotoxic to *mammalian* cells [17,19,38] and proceed through an oligodynamic effect [23] being in principle possible to be used to induce bacterial inactivation on implants in a way that it is not toxic to human health. The antibacterial effects of Cu-nanoparticulate films shown in Fig. 6b as well as for the case of Ag-nanoparticles films leaching Ag-species are due to Cu-ions and Ag-ions diffusing through the cell-wall porins into the cell core leading to cell death.

Fig. 6c in shows the methicillin resistant *S. aureus* (MRSA) inactivation in the dark by HIPIMS Cu-polyester sputtered with the same power (60 A) as applied in the samples used to inactivate bacteria (Fig. 6a). The times necessary to inactivate MRSA are similar to the times required to inactivate *E. coli* when starting with the same CFU bacterial concentration. This is not surprising since both involve the destruction of organic matter. This is an important observation with a wide application potential. Dark bacterial inactivation is important in hospital facilities. It also avoids the formation of pathogens biofilm formation leading to hospital acquired infections (HAI) as described in the first paragraph of the Introduction.

Table 3 shows the surface atomic composition % for the main elements on the Cu-polyester as a function of the bacterial inactivation time. The surface C in the films at time zero decreases with respect to pure polyester due to the sputtered Cu. When contacted with bacteria (Table 2, third column) the C-content in the sample is seen to decrease again due to the Cu-mediated bacterial degradation. At longer reaction
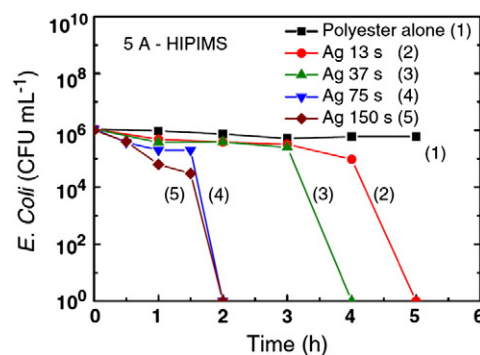

Fig. 3. Nominal calibration of the Cu thickness layers sputtered by HIPIMS at 6 A and 60 A.

Fig. 4. *E. coli* inactivation as a function of time for Ag-polyester sputtered at 5 A for different times in the dark.
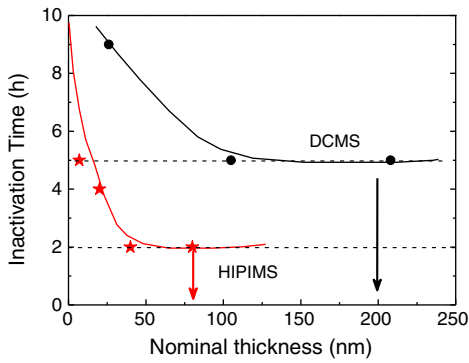
Fig. 5. Inactivation times as a function of the nominal thickness of the Ag-layers deposited by HIPIMS at 5 A and DCP at 0.3 A.
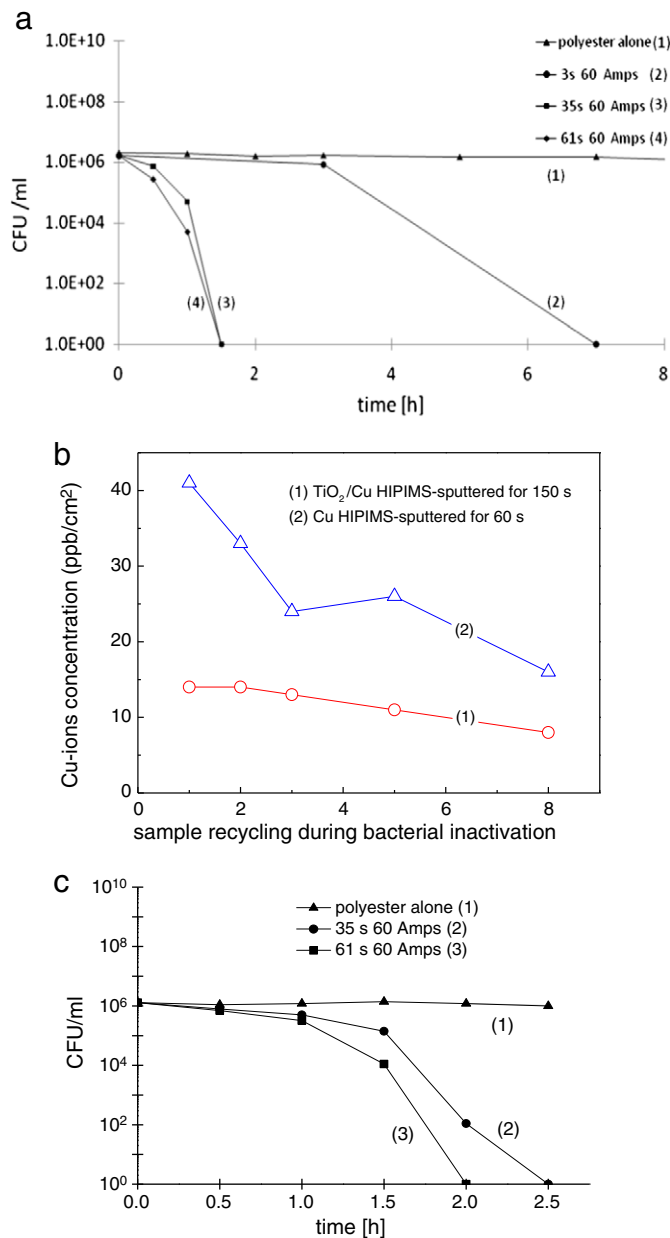

Fig. 6. a. Kinetics of *E. coli* inactivation in the dark mediated by Cu-polyester HIPIMS sputtered at 60 A. b. Concentration of ions eluted into solution determined by ICP-MS up to the 8th repetitive use of a TiO$_2$/Cu inactivating *E. coli* K-12. c. Kinetics of methicilin resistant *Staphylococcus aureus* (MRSA) inactivation by Cu-polyester fabrics HIPIMS sputtered at 60 A, in the dark.

times, the surface % of C-stabilizes due to the presence of death bacteria up to 90 min. The Cu % present is seen to decrease after time zero due to the presence of surface carbon up 90 min.

The XPS-spectrogram of the Cu-samples presented Cu(2p$_{3/2}$) and Cu(2p$_{1/2}$) peaks centered at 934.2 and 954.1 eV and this doublet is attributed to the presence of the Cu^{2+} oxidation state (Cu^{2+}) prevalent in the oxidized form of the Cu-sputtered sample exposed to air [35,39]. We suggest based on the evidence of the XPS data that the production of reactive oxygen species (ROS) inside *E. coli* leading to bacterial inactivation involves the redox catalysis Cu^{2+}/Cu^{1+} by reactions after contacting the bacteria in the dark as noted below

$$Cu^+ + O_2{}^{\cdot-} \leftrightarrow Cu^o + O_2 \qquad (6)$$

$$Cu^o + O_2 \leftrightarrow Cu^+ + O_2{}^{\cdot-} \qquad (7)$$
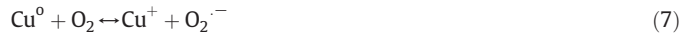
The Cu^{2+} is able to enhance the ROS formation via Fenton like reaction [39]

$$Cu^{2+} + e-_{cb} \leftrightarrow Cu^+ \qquad (8)$$

or by a two electron transfer from Cu^{2+} leading to Cu^o atoms

$$Cu^{2+} + 2e^- \leftrightarrow Cu^o \qquad (9)$$

The Cu-atoms then coalesce to Cu^o nanoparticles settling in the Cu-network of the polyester with $E_{redox} = -0.34$ V vs. NHE [40].

3.4. Ag and Cu-ions sputtered by HIPIMS and DCMS determined by mass spectroscopy (QMS)

Fig. 7 presents the ion-composition when sputtering Ag by HIPIMS in an Ar atmosphere by QMS. The Ag presents ionization potentials of 7.6 eV for Ag$^+$ and 21.5 eV for Ag^{2+} compared with the buffer gas Ar$^+$ of 15.7 eV. When increasing current, the amount of Ar$^+$-ions decreases and the Ag$^+$-ions in the gas phase increase. At discharge currents greater than 5 A, Ag$^+$-ions exceeded the amount of Ar$^+$-ions. The most interesting result was found for the 10 A peak current leading to high quantities of Ag$^+$-ions with a small amount of Ag^{2+}-ions. In the current experiments HIPIMS power densities are at least a factor of 4–10 higher compared to DCMS leading to a significant difference in the ion-flux composition in Fig. 7. The composition of HIPIMS at the lowest current of 1 A (current density of 20 mA/cm^2) was similar to the case of DCMS sputtering with a current of 300 mA (current density of 15.3 mA/cm^2). In the presence of O$_2$ the Ag^{2+}-ion leads to AgO [40].

Fig. 8 presents the ion-composition when sputtering Cu by direct current magnetron sputtering (DCMS) and HIPIMS in Ar-atmosphere from QMS analysis. The ionization potential of Cu$^+$ is 7.7 eV. By inspection of Fig. 8, the composition of the ions in the DCMS chamber gas phase was: 87% Ar$^+$, 5% Ar^{2+} and 8% Cu$^+$. Low amounts of Cu$^+$-ions were found for the DCMS-sputtered samples. The amount of Cu$^+$-ions increases with HIPIMS at 6 Amps to reach 97% along 3% Ar^{2+}. Finally, at 60 Amps the composition of the gas phase is: 17% Ar$^+$, 3% Ar^{2+}, 75% Cu$^+$ and 5% Cu^{2+} [41,42]. Because of the different power applied by HIPIMS the ion trajectory in the plasma and subsequent condensation on the substrate surface proceed with a different diffusion and condensation in the case of HIPIMS compared to DCMS. HIPIMS leads to less voids and denser films. In general the cluster size is reduced. But especially for Ag-HIPIMS there is literature showing that the opposite happens. It is expected that the percolation threshold will be reduced. Nevertheless the silver atoms and especially the ions tend to from clusters instead of growing a flat uniform film. Therefore the percolation happens later—at higher film thickness. This might be also one reason for the Ag-activity. Since the film is forming nanocrystalline clusters the effective surface area is increased (fractional surface). This leads to

Table 3
Surface atomic composition concentration % of the main elements on the polyester Cu-sputtered by HIPIMS for 60 s at 60 Amps.

| Sample	C	O	N	Cu	Na	P	Cl
Polyester blank	75.30	23.13			1.21	0.36	
Polyester + Cu, time zero	53.76	26.50		19.74			
Polyester + Cu + bacteria, time zero	44.81	32.63	0.48	14.08	2.80	2.19	0.31
Polyester + Cu + bacteria (30 min)	68.89	22.04	1.14	1.76	3.70	0.35	
Polyester + Cu + bacteria (60 min)	60.29	25.90	0.35	4.59	3.15	0.93	
Polyester + Cu + bacteria (90 min)	61.13	23.84	0.20	4.35	3.56	6.11	
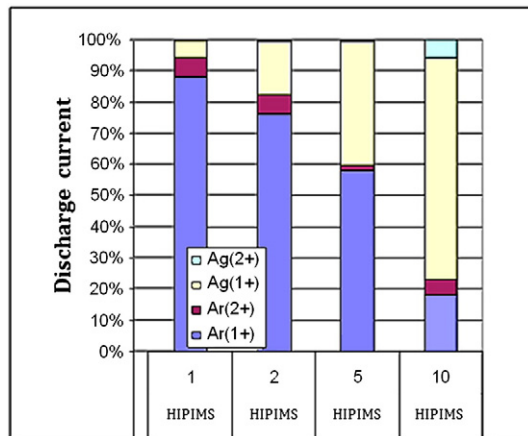
Fig. 7. Plasma ion-composition analysis of HIPIMS in argon, derived from mass spectroscopy analysis. HIPIMS is applied at different currents as indicated in the figure.

higher reactivity and possibly to higher cell death rate. Smaller metal lattice constants have been reported by XRD for the HIPIMS layers compared to DCMS layers usually deposited using lower energies [25–33].

The HIPIMS runs show that with increasing current, the Ar^{2+} and Cu^{2+} in the gas phase increase. During the magnetron sputtering chamber, the ionization $Ar \leftrightarrow Ar^+ + e^-$ leads in a subsequent step to the collision of the electron with $e^- + Cu^o \leftrightarrow Cu^+ + 2e^-$. The high-speed electron during the physical collision with the Cu kicks off a second electron leading to the Cu^+-ion. In the case of HIPIMS, the metal-ions with a higher e-density interact more readily with biased polyester in the magnetron chamber.

4. Conclusions

This study presents the surface functionalization of polyester by very thin sputtered Ag and Cu-layers inducing accelerate *E. coli* inactivation in the dark (minute range). The thin Ag and Cu films were uniform and presented adhesive properties and their stability led to repetitive loss of bacteria viability. A considerable saving in metal and deposition time (energy) was found for HIPIMS sputtered surfaces compared to conventional DCMS-sputtered surfaces. Increasing demand for Ag/Cu
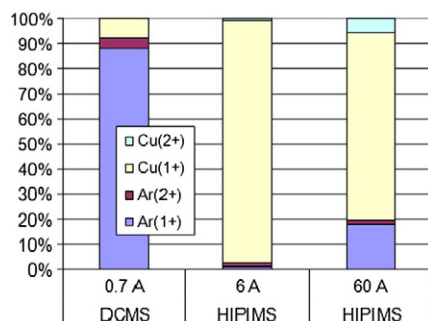
Fig. 8. Ar-ion composition and Cu-ion composition determined by mass spectrometry in the gas phase for a DCMS and a HIPIMS sputtering chamber. For other details see text.

is decreasing rapidly the known world reserves. This is important since both metals are strategically important metal. These films preclude biofilm formation spreading infectious bacteria of all sorts in hospitals, schools, and public places. The films developed in this study present a practical application potential for the preparation of a variety of disinfecting surfaces.

Acknowledgments

References

[1] A. Kramer, I. Schwebke, G. Kampf, BMC Infect. Dis. 6 (2006) 130–138.
[2] K. Taylor, R. Roberts, J. Roberts, The challenge of hospital acquired infections (HAI), Nat. Audit Office, 2002.
[3] K. Page, M. Wilson, I.P. Parkin, J. Mater. Chem. 12 (2009) 3819–3831.
[4] T. Yuranova, A. Rincon, A. Bozzi, S. Parra, C. Pulgarin, P. Albers, J. Kiwi, J. Photochem. Photobiol. A 161 (2003) 27–34.
[5] T. Yuranova, A. Rincon, C. Pulgarin, D. Laub, N. Xanthopoulos, H.-J. Mathieu, J. Kiwi, J. Photochem. Photobiol. A 181 (2006) 363–369.
[6] G. Borkow, J. Gabbay, J. FASEB (2008) 1728–1730.
[7] G. Borkow, J. Gabbay, Med. Hypotheses 70 (2008) 990–994.
[8] L. Zhang, R. Dillert, D. Bahnemann, M. Vormoor, Energy Environ. Sci. 5 (2012) 7491–7507.
[9] H. Foster, I. Ditta, S. Varghese, A. Steele, Appl. Microbiol. Biotechnol. 90 (2011) 1847–1868.
[10] H.M. Yates, L.A. Brook, I.B. Ditta, P. Evans, H.A. Foster, D.W. Sheel, A. Steele, J. Photochem. Photobiol. A 197 (2008) 197–2005.
[11] J. Musil, M. Louda, R. Cesrtvy, P. Baroch, I.B. Ditta, A. Steele, H.A. Foster, Nanoscale Res. Lett. 4 (2009) 313–320.
[12] L.A. Brook, P. Evans, H.A. Foster, M.E. Pemble, A. Steele, D.W. Sheel, H.M. Yates, J. Photochem Photobiol. A 187 (2007) 53–63.
[13] I. Sondi, S. Sondi, J. Colloid Interf. Sci. 275 (2004) 177–182.
[14] P.V. Ashrani, G.L. Mun, M.P. Hande, S. Valyaveettil, ACS Nano 3 (2009) 279–290.
[15] J. Liu, D. Sonshine, S. Shervani, R. Hurt, ACS Nano 4 (2010) 6903–6913.
[16] S. Dancer, J. Hosp. Infect. 73 (2009) 378–385.
[17] F. Heidenau, W. Mittelmeier, R. Detsch, M. Haenle, F. Stenzel, G. Ziegler, H.A. Gollwitzer, J. Mater. Sci. Med J. Mater. Sci. Med. 16 (2005) 883–889.
[18] T. Ehirai, H. Tsuchiya, T. Shimizu, K. Ohtani, Y. Zen, K. Tomita, J. Biomed. Mater. Res. B Appl. Biomater. 91 (2009) 373–380.
[19] M. Haenle, A. Fritsche, C. Zietz, R. Bader, F. Heidenau, W. Mittelmeier, H. Gollwitzer, Mater. Sci. Mater. Med. 22 (2011) 381–387.
[20] K. Sunada, S. Watanabe, K. Hashimoto, Environ. Sci. Technol. 40 (2003) 4785–4789.
[21] J. Kiwi, C. Pulgarin, Catal. Today 151 (2001) 2–7.
[22] A. Torres, C. Ruales, C. Pulgarin, A. Aimable, P. Bowen, J. Kiwi, Appl. Mater. Interfaces 1 (2010) 2547–2552 (65 m2/g).
[23] Thüringer Surface and Biomaterials Kolloquium, Zeulenroda, Germany, 13–15 September 2011.
[24] 22nd Annual BioInterface Conference 2012, University College Dublin, Ireland, October 23–25 2012.
[25] J. Lin, J. Moore, W. Sproul, B. Mishra, Z. Wu, L. Wang, Surf. Coat. Technol. 204 (2010) 2230–2239.
[26] K. Sarakinos, J. Alami, D. Konstantinidis, Surf. Coat. Technol. 204 (2010) 1661–1684.
[27] A. Petrov, J. Myers, E. Greene, J.R. Abelson, J. Vac. Sci. Technol. A 12 (1994) 2846–2851.
[28] J. Alami, P. Persson, J. Gudmunsoon, J. Bohlmark, J. Helmersson, J. Vac. Technol. A 23 (2005) 278–280.
[29] V. Kousznetsov, K. Macak, J. Schneider, U. Helmersson, I. Petrov, Surf. Coat. Technol. 12 (1999) 290–295.
[30] A. Ehiasarian, Pure Appl. Chem. 82 (2010) 1247–1258.
[31] A. Ehiasarian, A. Vetushka, A. Hecimovic, l S. Konstantinidis, J. Appl. Phys. 104 (2008) 083305.

[32] A. Ehiasarian, Y. Gonzalvo, T. Whitmore, Plasma Process. Polym. 4 (2007) 5309–5313.
[33] Laura Rio, Ewelina Kusiak, John Kiwi, César Pulgarin, Andrej Trampuz, Alain Bizzini, Appl. Environ. Microbiol. 78 (2012) 8176–8182.
[34] D. Briggs, M. Shea, Practical Surface Analysis, 2nd edition, Auger and X- rays, vol. 1, John Wiley & Sons, Chichester, New York, Toronto, Singapore, 1988.
[35] C. Wagner, M. Riggs, E. Davis, G. Mullenberg, E. G (Eds.), Handbook of X-Ray Photo-electron Spectroscopy, Perkin-Elmer Corp. Physical Electronics Division, Minnesota, 1979.
[36] A.D. Shirley, Phys. Rev. B5 (1972) 4709–4716.
[37] J.W. Mathews, Epitaxial growth, Part B, Ch 4: Nucleation and Thin Films, Academic Press, New York, 1975. 382.
[38] M. Heinlaan, I. Blinova, H.-C. Dubourguier, A. Kahru, Chemosphere 71 (2008) 1308–1316.
[39] G. Biederman, G. Sillen, Acta Chem. Scand. Part 3014 (1969) 14–0717.
[40] O. Baghriche, A.P. Ehiasarian, E. Kusiak-Nejman, A.W. Morawski, C. Pulgarin, R. Sanjines, J. Kiwi, J. Photochem. Photobiol. A 227 (2012) 11–17.
[41] O. Baghriche, R. Sanjines, C. Pulgarin, S. Rtimi, J. Kiwi, J. Photochem. Photobiol. A 251 (2013) 50–56.
[42] E. Kusiak-Nejman, A.W. Morawski, A.P. Ehiasarian, O. Baghriche, C. Pulgarin, E. Mielczarski, J. Mielczarski, A. Kulik, J. Kiwi, J. Phys. Chem. C 115 (2011) 21113–21119.